Predicting crystallization-dependent residual stress development in thermoplastic composites

Nithin K. Parambil[1]*, Branndon R. Chen[1], Joseph M. Deitzel[1] and John W. Gillespie Jr.[1]
[1] University of Delaware, Center for Composite Materials, 101 Academy Street, Newark, DE 19720, USA.
*Corresponding Author: nithinkp@udel.edu

Abstract

Fiber reinforced thermoplastic composites are attractive for automotive applications due to their increased throughput potential over their thermosetting counterparts. Understanding and predicting thermal residual stress is a key factor in designing components to maximize performance by reducing warpage/defects and optimizing the processing method. Thermal residual stress, resulting from the coefficient of thermal expansion (CTE) mismatch of the matrix and fiber, can be significant because of the large thermal gradients between melt/processing and service temperatures. Further residual stress can be induced upon crystallization if the matrix exhibits crystalline/semi-crystalline behavior. A computational model predicting the process-induced residual stress is developed for AS4/polypropylene micro-composites and implemented via user material subroutine (UMAT) in ABAQUS. The model includes the cooling-rate dependent crystallization, temperature-dependent elastic modulus, and temperature-dependent CTE of the matrix, and the temperature-independent transversely isotropic properties of carbon fiber and can replicate the experimental conditions (initial fiber preload to prevent buckling) and process history. Post-process, micro-Raman spectroscopy is utilized to validate and quantify the residual strain developed in the fiber for different preload (1 – 8 g) far away from the free edge of the sample. The measured compressive strain values show a good correlation with the FE predicted residual strain for various preload conditions.

Keywords: *residual stress, crystallization, Raman spectroscopy, carbon fiber*

Introduction

In the last decades thermoplastic composites (TPCs) gain traction over thermoset composites due to their high throughput [1]. Thermoplastics are well known for toughness, weldability, chemical resistance, recyclability, etc. Carbon fiber reinforced polypropylene provides higher specific stiffness and strength than glass fiber composites and offers higher weight savings for various applications such as automotive, construction, and consumer products [2][3]. However, due to mismatch in the coefficient of thermal expansion (CTE) between the matrix and the fiber and the formation of crystals due to the crystallization of polypropylene result in the thermal residual stresses during processing from relatively high process temperature and cooling rates [4]. Additional loading on the microstructure can be induced due to the mismatch in CTE between layers of different ply orientations and non-isothermal cooling of the layers (thermal gradients through thickness that vary with time). Crystallization shrinkage can also contribute to volumetric shrinkage and residual stress in the case of semicrystalline polymers such as polypropylene [5]. Residual stress results in loss of dimensional stability/warpage and reduced assembly tolerance as well as contribute to the microstructural damage due to static and fatigue loading of the structure.

The prediction and validation of residual stress development in AS4 carbon fiber in a polypropylene (PP) matrix at the microstructural length scale is the focus of this paper. In the previous study, we made a simplifying assumption to define the stress–free temperature (Tsf) as the end of the crystallization temperature (cooling rate dependent) for the residual stress calculations [6] [7]. In the present study, we relax this assumption by starting the residual stress calculation in the melt and include non-isothermal crystallization effects to predict processing-induced residual stress. PP's cooling-rate-dependent crystallinity, temperature-dependent elastic modulus, temperature-dependent coefficient of thermal expansion (CTE), crystallization-dependent shrinkage, and CTE and CTE mismatch of PP and carbon fiber (AS4) are measured and modeled to predict the residual stress as a function of process history.

Experimental comparison is required for the validation of the model developed. There are many experimental methods are available in the literature for measuring the strain in the composite. But at the fiber length scale (diameter of carbon fiber is ~7 μm), Raman spectroscopy has been proved to be a better technique to measure the in-situ fiber strain states [8] [9]. Residual stress predicted at different preloads (pre-defined weight at the end of fiber ends) was validated using the Raman spectroscopy method in the present study.

Resin Thermal and Mechanical Properties Characterization

PP is a semi-crystalline polymer; the cooling rate affects the crystallization behavior and thus affects the resulting microstructure which in turn has a significant effect on the ultimate properties of the matrix and composite material. The relationship between Young's modulus and crystallinity of isotactic polypropylene (iPP) under the influence of different service temperatures is shown in Figure 1 from the literature [10]. Since the crystals are embedded in the amorphous iPP, it follows a constant stress condition. The inverse rule of mixture (IROM) is used to calculate the temperature-dependent amorphous modulus and obtained the crystal modulus value as ~6300 MPa [10] [11]. Figure 1 compares the temperature-dependent modulus versus crystallinity with literature and the inverse rule of mixture (IROM). IROM is a good assumption to model crystallinity and temperature-dependent modulus.

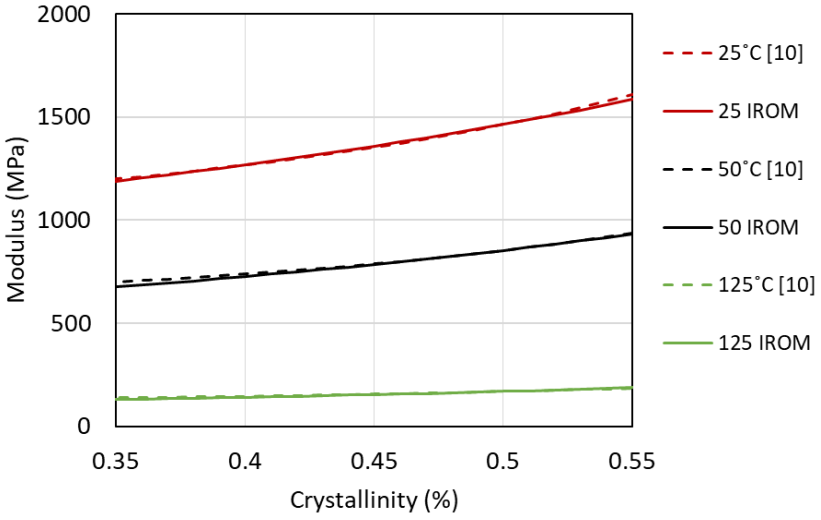

Figure 1. Comparing temperature-dependent modulus versus crystallinity with literature and inverse rule of mixture (IROM).

The Young's modulus at different temperatures (strain rate of 1e-4 s^{-1} and 50% crystallinity) is shown in Figure 2. In Figure 2 experimental results are fitted with exponential law. Using IROM and inputting crystal modulus, temperature-dependent amorphous modulus has been calculated. The modulus in the melt above the onset of crystallization is assumed to be zero. Crystallization prediction versus time for the thermal histories in the single-fiber thin film sample is shown in Figure 3. Inputting the temperature and cooling rate dependent crystallinity and amorphous modulus, crystallinity and cooling rate dependent resin modulus is calculated using IROM and is shown in Figure 4. For the case of 50% crystallinity, the temperature-dependent modulus is shown in Figure 2. Figure 4 shows the temperature-dependent modulus including crystallization effects using the thermal history given in Figure 2.

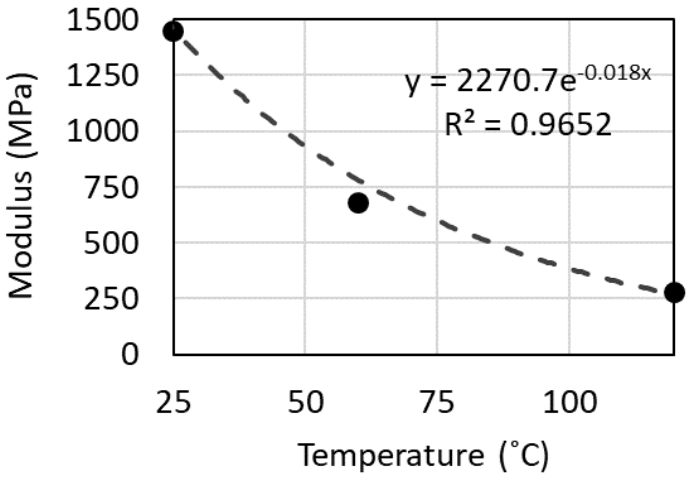

Figure 2. Modulus versus temperatures at a strain rate of 1e-4 s^{-1} and 50% crystallinity (Dots – experiment, dash lines – fitting) [7].

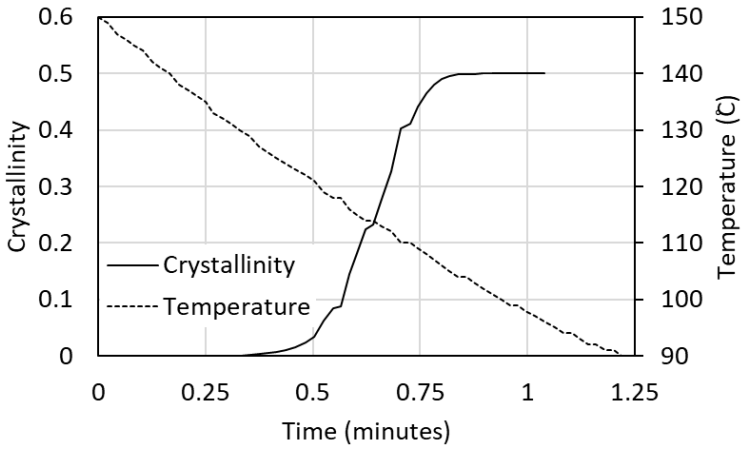

Figure 3. Crystallization prediction versus time for the thermal histories in the single-fiber thin film sample [7].

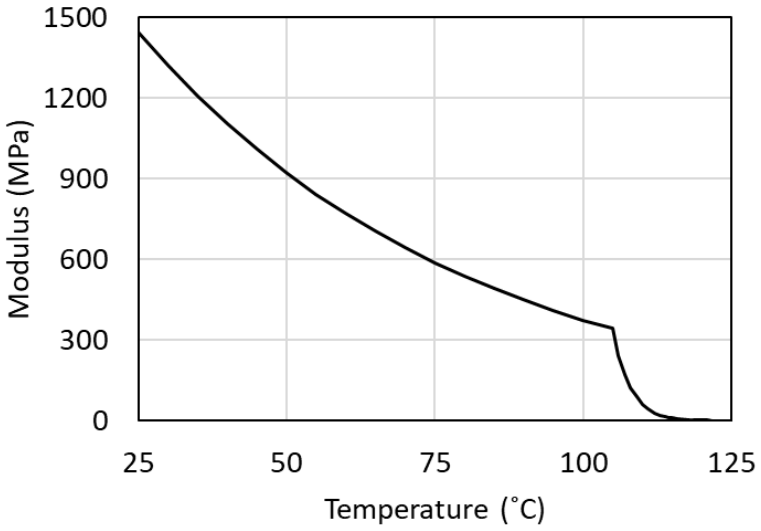

Figure 4. Temperature-dependent modulus for the thermal history is shown in Figure 3.

The isotropic shrinkage strain of a unit volume element of resin, $\Delta\varepsilon_r^{cry}$, resulting from an incremental volume resin shrinkage, ΔV_r^{cry}, may be calculated as [12] [13]:

$$\Delta\varepsilon_r^{cry} = \frac{-1+\sqrt{1+4/3\Delta V_r^{cry}}}{2}$$

The incremental volume resin shrinkage computed for each time increment is calculated by the ratios of instantaneous densities based on instantaneous crystallinity:

$$\Delta V_r^{cry} = \frac{\rho(X_c)_{t-1} - \rho(X_c)_t}{\rho(X_c)_t}$$

The resin density at the current time increment is calculated using the equation as $\rho_m = \rho_c V_c + (1 - V_c)\rho_a$ (ρ_c = 946 kg/cm^3, ρ_a = 855 kg/cm^3).

The incremental thermal shrinkage strain is determined from the instantaneous, temperature-dependent resin thermal expansion coefficients and the temperature increment between time steps, as,

$$\Delta\epsilon^{cte} = \alpha(T).\Delta T$$

The total processing-induced resin shrinkage, $\Delta\epsilon^{th} = \Delta\varepsilon_r^{cry} + \Delta\epsilon^{cte}$. In Figure 5, the total processing-induced resin shrinkage strain for different cooling rates is shown.

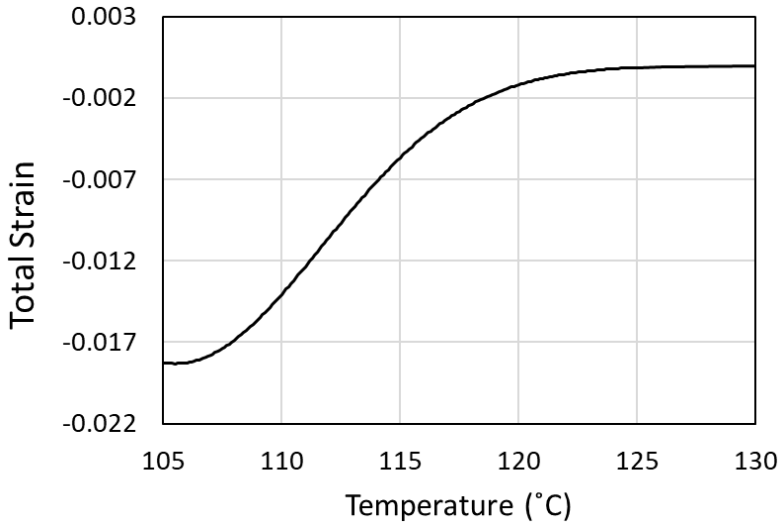

Figure 5. The predicted total processing-induced resin shrinkage strain for the thermal history is given in Figure 3.

The effective CTE at the crystallization shrinkage can be calculated from the total processing-induced resin shrinkage strain. The total processing-induced resin shrinkage, $\Delta\epsilon^{th} = \alpha_{\text{eff}}(T).\Delta T$ as shown in Figure 5. The effective CTE during processing induced resin shrinkage is $\alpha_{\text{eff}}(T) = \frac{\Delta\epsilon^{th}}{\Delta T}$ and as shown in Figure 6.

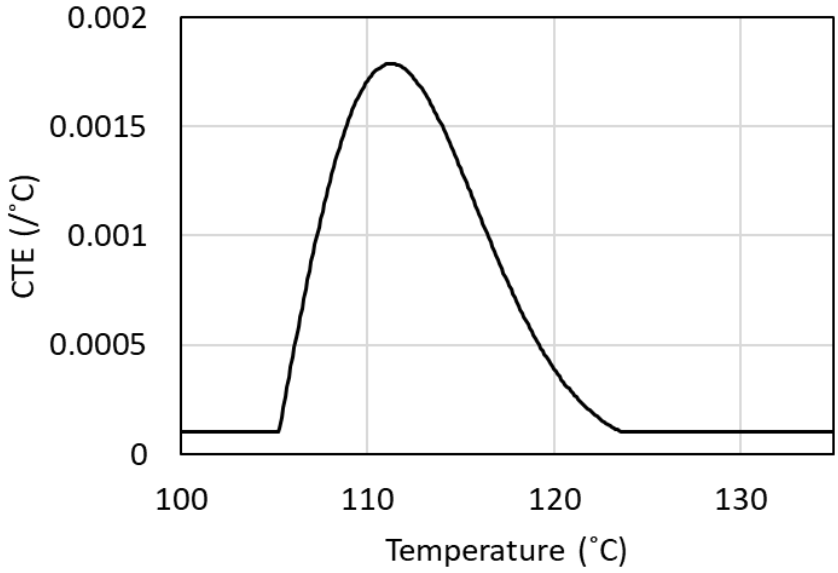

Figure 6. The effective CTE during processing induced resin shrinkage (CTE after crystallization is 1e-4 /˚C).

Polypropylene Constitutive Model

UMAT in ABAQUS has been developed for constitutive properties for PP to incorporate the effects of cooling-rate dependent crystallinity from the melt to the room temperature on the temperature-dependent and crystallinity-dependent Young's modulus, and temperature-dependent

shrinkage strains (crystallization shrinkage and thermal expansion. A detailed description of the constitutive model is given in [6] and [7].

Prediction and Validation of Micro-Composite Residual Stress

A FE model incorporating the developed UMAT has been used to predict residual stress developed in a single fiber fragmentation test (SFFT) specimen from melting temperature to room temperature (including all processing conditions). We validate the predicted axial strain in the fiber using Micro-Raman spectroscopy to measure the fiber strain in the SFFT specimen at room temperature. Additional validation is provided by varying fiber pretension in both the models and experiments. Fiber pretension is achieved by applying preload (a measured weight at the fiber ends) to the fiber during the fabrication of the SFFT samples. This is commonly done during SFFT testing to minimize the waviness in the fiber due to the mismatch in axial shrinkage between the fiber and matrix. In the present study, fiber pretension alters the axial strain of the fiber after processing and provides an opportunity to validate the model over a wide range. The compressive fiber strain is reduced due to the increase in the preload.

Single Fiber Sample Preparation

Optically transparent and uniform thickness SFFT samples are needed to observe under the Micro-Raman technique and match with FE model geometry. Thin 100 μm films were obtained by hot pressing the polypropylene pellets. Two precision ground aluminum plates lined with Kapton films were used to press the as-received polypropylene pellets. The aluminum plate stack was hot-pressed in a Carver press with 6x6 at 220°C, a slight pressure of 1000lbs was applied to achieve the desired thickness with the shims. Then the setup is air-cooled (thermal history as shown in Figure 3) to room temperature.

Single AS4 fibers are separated and placed between two PP thin sheets. This stack of sheets was placed between two Kapton-lined aluminum caul plates. AS4 fiber with preload weight on the fiber ends (1 – 8 g) sandwiched between the thin PP film is hot pressed at 220˚C for 10 minutes. Next, the sample is forced to air cool to room temperature, and preload weights and Kapton sheets were removed from the sample (see Figure 3). Given the inherent uncertainty in the Raman strain measurement technique, the applied preload levels have to be large enough so that measured strains are discernable [14] [15]. Ultimately 1 – 8g preloads were sufficient for the validation experiments. The typical failure load of the AS4 carbon fiber was 15 - 17 g.

FE Model to Predict Micro-Composite Residual Stress

To predict the residual stresses in micro-model composites accurate FE models of experiments are required. SFFT specimen is the simplest case of a model composite that has been modeled in an account of the experimental dimensions. Carbon fiber has been modeled as a transversely isotropic elastic material with different CTE in the longitudinal and transverse directions as shown in Table 1.

Table 1. Material properties for AS4 carbon fiber [16] [17].

Elastic constants	E11 (GPa)	E22 (GPa)	ν12	ν23	G12 (GPa)	G23 (GPa)	α11 (μstrain/˚C)	α22 (μstrain/˚C)

AS4 Carbon fiber	235	14	0.2	0.25	2.8	5.6	-1.2	5.5

The FE model replicated the experimental steps as follows:

1. At melt processing temperature fiber preload is
2. From the melting temperature to room temperature the system cools down with the preloads
3. At room temperature removed the preload

Figure 7. FE model for single fiber fragmentation (t/d ≈ 14.5, L/d ≈ 285).

Micro-composite model has been generated for the analysis as shown in Figure 7 as a quarter-symmetric model. A mesh size of 2μm is obtained as the converged mesh after the mesh convergence study (by changing the mesh size from 3 – 0.75 μm). A symmetry boundary condition is applied to the plane y = 0 and z = 0. The stress-free boundary condition is applied to the plane y = B/2 and z = t/2. After removing preload of 1g considering Tsf = 150˚C (melt temperature), residual strain is measured and shown in Figure 8. Due to the end effects, the shear–lag strain distribution is visible in Figure 8. The residual axial strain considering E independent of T and E function of T is shown in Figure 8. Most of the literature assumes E independent T [18] [19] for measuring residual stress and over-predicts the stresses and strain. Figure 8 clearly shows the importance of including temperature-dependent properties.

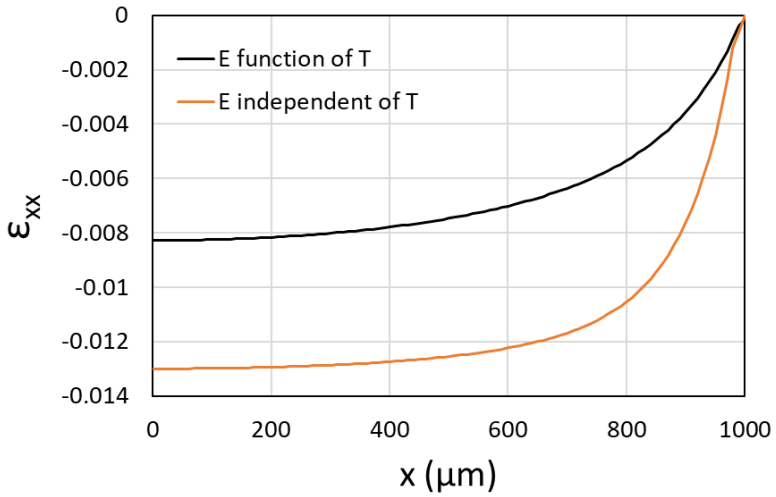

Figure 8. the residual axial strain considering E independent of T and E function of T.

Figure 9 shows the residual stress calculation considering the simplified assumption that Tsf is defined as the temperature at the end of (cooling rate dependent) and the present study starts in the amorphous melt and includes all non-isothermal effects of temperature and crystallization kinetics on modulus and shrinkage. The predicted residual stress between the two approaches is within 5% variation. In the case of PP that undergoes 50% crystallization shrinkage, the correlation shows that the approach defining the Tsf as the temperature at the end of crystallization is accurate. A key feature of this approach is to recognize that the temperature at the end of crystallization is cooling rate dependent. Slow cooling rates have a higher stress-free temperature (resulting in higher residual stress) than fast-cooling rates (lower residual stress). In the case of PP, the final crystallinity for all cooling rates is approximately 50%. The contribution of crystallization shrinkage to residual stress is small since the modulus of PP during crystallization is also small.

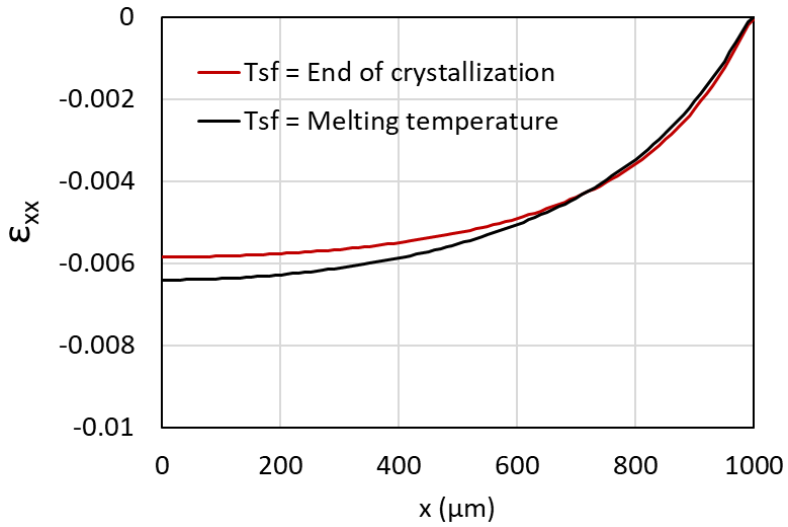

Figure 9. ε_{xx} along the length of the fiber after removing preload 4g (Free fiber end at 1000μm) with Tsf as the end of crystallization and melting temperature.

Raman Measurement Results

A strain versus Raman peak shift calibration curve was generated for AS4 fibers using a Renishaw Qontor Raman microscope. Carbon fibers with different processing-applied preload were observed in the matrix using the calibration curve. Comparing the bulk residual strain in the micro-composite with the FE model was a good metric for validation. Both experimental and model measurement was made far away from the end of the SFFT specimen to avoid end effects. There was a good correlation between the FE model and the experiment for all three preload cases (1g, 4g, and 8g) and are with1g, 4g, and 8g in the standard variation of the experiments as shown in Figure 10. This is a good indication that the FE model and experimental inputs are mimicking the physical specimens we can produce experimentally.

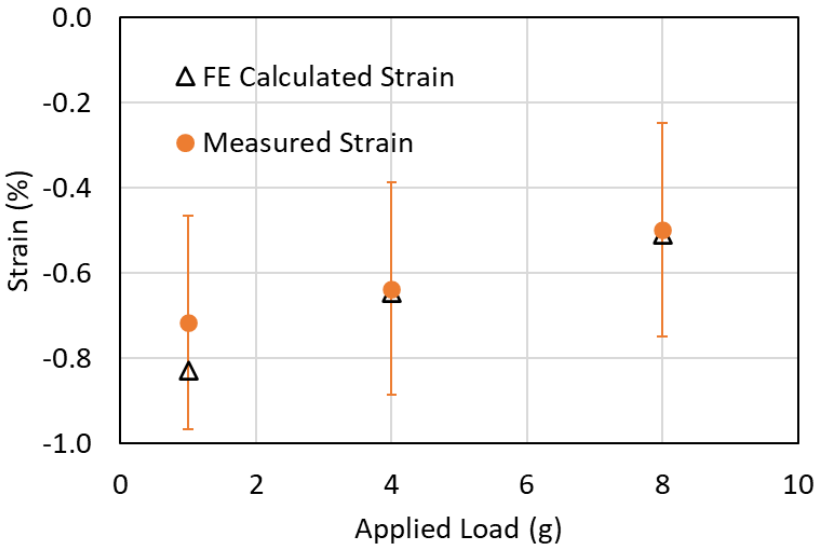

Figure 10. Bulk-level FE calculated residual strain for given preload conditions compared with experimentally measured values (1000μm from the edge).

Conclusion and Future Work

FE model residual stress predictions including the thermal and mechanical preloading show a good correlation with the experimental Raman strain measurements in the bulk. These methods provide more accurate residual stress by including the temperature-dependent crystallization modulus build-up from melting temperature to room temperature. However, the previous simplified approach of considering Tsf as the end of crystallization is within a 5% variation of this more complex modeling approach. We can apply this methodology to more complicated geometries, such as the pullout test geometry where residual stress plays an important role in the mechanical response once validated in a simple case.

Acknowledgments

This research was sponsored by the National Aeronautics and Space Administration under Grant and Cooperative Agreement No. 80NSSC20M0164, issued through the Aeronautics Research Mission Directorate, Transformative Aeronautics Concepts Program, University Leadership Initiative.

References

[1] Parlevliet PP, Bersee HEN, Beukers A. Residual stresses in thermoplastic composites—A study of the literature—Part II: Experimental techniques. Composites. Part A, Applied science and manufacturing 2007;38(3):651-665.

[2] Gillespie JW, Chapman TJ. The Influence of Residual Stresses on Mode I Interlaminar Fracture of Thermoplastic Composites. Journal of Thermoplastic Composite Materials 1993;6(2):160-174.

[3] Parlevliet PP, Bersee HEN, Beukers A. Residual stresses in thermoplastic composites—A study of the literature—Part I: Formation of residual stresses. Composites. Part A, Applied science and manufacturing 2006;37(11):1847-1857.

[4] Parlevliet PP, Bersee HEN, Beukers A. Residual stresses in thermoplastic composites – a study of the literature. Part III: Effects of thermal residual stresses. Composites. Part A, Applied Science and Manufacturing 2007;38(6):1581-1596.

[5] Chapman TJ, Gillespie JW, Pipes RB, Manson J-E, Seferis JC. Prediction of Process-Induced Residual Stresses in Thermoplastic Composites. Journal of Composite Materials 1990;24(6):616-643.

[6] Parambil NK, Chen BR, Deitzel JM, Gillespie JR JW, Vo, LT and Sarosi, P. Predicting Processing Induced Residual-Stresses in Carbon Fiber-Thermoplastic Micro-Composites, Proceedings of the American Society for Composites—Thirty-Sixth Technical Conference on Composite Materials, 2021
.

[7] Parambil NK, Chen BR, Deitzel JM, Gillespie JW. A methodology for predicting processing induced thermal residual stress in thermoplastic composite at the microscale. Composites. Part B, Engineering 2022;231:109562.

[8] Huang Y, Young RJ. Effect of fibre microstructure upon the modulus of PAN- and pitch-based carbon fibres. Carbon (New York) 1995;33(2):97-107.

[9] Qian X, Wang X, Zhong J, Zhi J, Heng F, Zhang Y, Song S. Effect of fiber microstructure studied by Raman spectroscopy upon the mechanical properties of carbon fibers. Journal of Raman spectroscopy 2019;50(5):665-673.

[10] Li J, Zhu Z, Li T, Peng X, Jiang S, Turng L. Quantification of the Young's modulus for polypropylene: Influence of initial crystallinity and service temperature. J Appl Polym Sci 2019;137(16).

[11] Menyhard A, Suba P, Laszlo Z, Fekete HM, Mester AO, Horvath Z, Voros G, Varga J, Moczo J. Direct correlation between modulus and the crystalline structure in isotactic polypropylene. Express polymer letters 2015;9(3):308-320.

[12] Lawrence WE, Seferis JC, Gillespie Jr JW. Material response of a semicrystalline thermoplastic polymer and composite in relation to process cooling history. Polymer Composites 1992;13(2):86-96.

[13] Eduljee RF, Gillespie Jr JW, McCullough RL. Residual stress development in neat poly(etheretherketone). Polymer engineering and science 1994;34(6):500-506.

[14] Huang Y, Young RJ. Effect of fibre microstructure upon the modulus of PAN- and pitch-based carbon fibres. Carbon (New York) 1995;33(2):97-107.

[15] Qian X, Wang X, Zhong J, Zhi J, Heng F, Zhang Y, Song S. Effect of fiber microstructure studied by Raman spectroscopy upon the mechanical properties of carbon fibers. Journal of Raman Spectroscopy 2019;50(5):665-673.

[16] Parambil NK, Gururaja S. Micro-scale progressive damage development in polymer composites under longitudinal loading. Mechanics of Materials 2017;111(1):21-34.

[17] Parambil NK, Gururaja S. Micromechanical damage analysis in laminated composites with randomly distributed fibers. Journal of composite materials 2016;50(21):2911-2924.

[18] Nairn JA. Analytical Fracture Mechanics Analysis of the Pull-Out Test Including the Effects of Friction and Thermal Stresses. Advanced Composites Letters 2000;9(6):373-383.

[19] Zhandarov S, Mäder E. Analysis of a pull-out test with real specimen geometry. Part II: the effect of meniscus. Journal of Adhesion Science and Technology 2013;28(1).